Broadening of the Rb resonance lines by the noble gases*

Ch. Ottinger,† Richard Scheps, G. W. York, and Alan Gallagher‡
Joint Institute for Laboratory Astrophysics, University of Colorado and National Bureau of Standards, Boulder, Colorado 80302
(Received 10 October 1974)

Normalized emission spectra of the optically excited Rb resonance lines (7800 Å, 7948 Å) have been measured in the presence of He, Ne, Ar, Kr, and Xe for about 50 Å on either side of the lines. The perturber gas pressures were in the range 100–1100 Torr and the temperature was 318 °K. The spectra, normalized to the total emission, are shown to be due to binary collisions. Shifts and widths of the Lorentzian cores of the lines were obtained, at pressures sufficiently low for impact theory to apply. The widths are corrected for the Rb hfs and the instrument function. Various power-law fits to the near-wing intensities are presented and compared to theoretical expectations. The red satellites reported by other authors are found to be, in the low-pressure limit, mere shoulders on the line wing for Ar and Kr, while Xe barely produces an actual peak. The measured linewidths and shifts are compared to previous measurements.

I. INTRODUCTION

The broadening of atomic lines due to neutral-gas collisions has been studied throughout this century.[1,2] It has long been recognized that the shapes of collisionally broadened lines can be related to the interaction potentials of the colliding species, particularly by use of the impact approximation in the core of the line and the quasistatic approximation in the far wings.[1] The impact approximation predicts for isolated lines a Lorentzian core of the line with a shift and width that are related primarily to the long-range interaction potentials. The relationship is, however, decidedly nonunique, so that measurements of this shift and width can be used to check a theoretical prediction but not to infer interaction potentials. The far-wing intensity, on the other hand, is very closely related to the close-range interaction potentials through the quasistatic theory. A measurement of the far-wing spectrum yields a very stringent constraint on these potentials.

In order to realize the full value of the information contained in the far-wing spectrum, it must be measured in absolute units. In an absorption experiment this means the wing absorption coefficient must be measured at known absorber and perturber densities, while in an emission measurement the wing intensity relative to the integrated emission must be measured. The quasistatic theory relates the normalized, binary wing intensity at $\lambda \to \lambda + d\lambda$ to the statistical probability $(g_j/g_A) n 4\pi R^2 dR \exp(-V/kT)$ that a perturber is in the differential volume $R \to R + dR$ about the radiator (g_j and g_A are the statistical weights of the molecular and parent atomic states and n is the perturber number density). (In order to apply the quasistatic theory, the frequency shift must be large, corresponding to close-range interactions. This statistical probability is small at the pressures corresponding to binary interactions.) The relationship between R and λ is fixed by $V^*(R) - V(R) = hc/\lambda$, the photon energy, where $V^*(R)$ and $V(R)$ are the adiabatic interaction potentials for the upper and lower states.[1] Thus, the actual wing intensity is needed to establish the relation $\lambda(R)$; a large $\lambda \to \lambda + \Delta\lambda$ wing intensity requires a large $R \to R + \Delta R$ differential volume and vice versa. Unfortunately, it has been traditional to study far-wing features, particularly "satellites" or local intensity maxima, but not to measure intensities. Thus the actual range or differential volume corresponding to the feature is undetermined, and it is not possible to deduce or test interaction potentials with any degree of certainty. If a satellite is observed in a far wing, this indicates that $V^*(R) - V(R)$ reached an extremum at about the satellite photon energy. Unless the entire wing-intensity pattern is measured, however, very little else can be reliably inferred about the potentials. In the absence of potentials it is difficult to study the accuracy of the approximations used in interpreting collisionally broadened spectra. For these reasons we have carried out the quantitative wing-intensity measurements reported here. In the interest of completeness we have also measured the shift and width of the Lorentzian portion of the line core and detected where the transition to non-Lorentzian shape occurs as a function of pressure and perturber specie.

In the present experiment the resonance-fluorescence spectrum is observed from optically excited Rb in a cell containing noble gas. The Rb density is low (~10^{-6} Torr) and varied so that the emission intensities relative to integrated emission can be obtained free from radiation entrapment, which attenuates the line center. The emit-

ting Rb state is selected by filtering the exciting radiation, and a double-grating monochromator is used to ensure spectral purity of the detected fluorescence. The present measurements are only extended to about 50 Å from the lines since quantitative measurements at greater separations have already been reported.[3] The measured line-center shapes are complicated by the smearing due to the spectrometer instrument function, the Rb hyperfine structure (hfs), and the Doppler width. To obtain the Lorentzian contribution to the observed spectral profiles, we have compared measured shapes to assumed spectral profiles obtained by convolution of the instrument function with Doppler and Lorentz broadened (Voigt) line shapes from each hfs component. This comparison has shown the point at which the line wing becomes non-Lorentzian at each pressure. From this information, the apparently nonlinear broadening that has been reported for some cases can be explained. Also, it becomes apparent that the widths and shifts of alkali resonance lines measured with many atmospheres of heavy noble-gas perturbers cannot be directly identified with the impact-broadened Lorentzian line.

II. THE EXPERIMENT AND RESULTS

A cell containing ~10^{-6} Torr of Rb and 0–1100 Torr of noble gas was illuminated by light from a Rb resonance lamp, filtered by $P_{1/2}$ or $P_{3/2}$ line interference filters. (The $5\,^2P_{3/2}$-$5\,^2S_{1/2}$, $\lambda = 7800$ Å, D_2 line will be labeled $P_{3/2}$; the $5\,^2P_{1/2}$-$5\,^2S_{1/2}$, $\lambda = 7948$ Å, D_1 line will be labeled $P_{1/2}$.) The fluorescence spectrum from the cell is filtered by a double grating monochromator and detected with a photomultiplier. In order to correct for small drifts, the integrated fluorescence from the cell was measured simultaneously by means of a second multiplier, the "fluorescence monitor." A schematic diagram of the apparatus and a discussion of gas handling and optical details, except for a change in spectrometer, can be found in Refs. 3 and 4. The cell temperature in the present experiments was 46 ± 6 °C, but the Rb density was maintained below the equilibrium vapor pressure. The methods used to adjust and monitor Rb density are also discussed in Refs. 3 and 4. The region of ±50 Å around each Rb line was scanned by the monochromator, with neutral-density filters inserted in the immediate vicinity of the line center in order to avoid saturation and nonlinearities in the photomultiplier current. The relative spectral sensitivity of the spectrometer plus photomultiplier was obtained by scanning a blackbody spectrum of known temperature.

The emission intensity varies rapidly near line center, where it is strongest, and more gradually in the wings, where it is weaker. Therefore, high-resolution data are needed near line center, while lower-resolution data can be used in the wings. Further, since the detected wing intensity varies as the square of the spectrometer slit width, it is advantageous in terms of the signal-to-noise ratio to use lower-resolution data in the wings. Consequently, spectrometer scans were taken with 10-, 50-, and 200-μm spectrometer slits, corresponding to measured instrument functions with half-widths of 0.12, 0.25, and 1 Å. The spectral regions covered by the 10-, 50-, and 200-μm slit settings were typically $|\Delta\lambda| = 3$, 8, and 100 Å, respectively. The intensity $I(\lambda)$ measured for each scan was divided by the integrated emission for that scan, $\int I(\lambda)\,d\lambda$. (Less than 1% of the area was neglected by integrating to ~20 Å either side of the line.) The resulting normalized emission spectra (units Å^{-1}) were plotted against the shift $\Delta\lambda$ or Δk from line center ($k = \lambda^{-1}$). An example is shown in Fig. 1. Far from the line

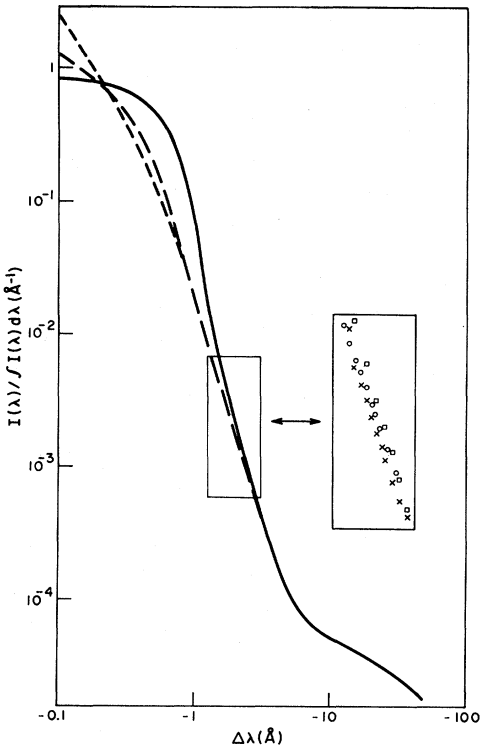

FIG. 1. Effect of instrumental resolution on measured line profiles. As an example, the blue wing of the Rb $P_{3/2}$ emission line, broadened by 300 Torr of Kr is shown. The three monochromator slit widths used were 10 μm (--- and × points), 50 μm (– – and ○) and 200 μm (—— and □), corresponding to a resolution of 0.12, 0.25, and 1 Å FWHM, respectively. Each scan is independently normalized to the total emission intensity $\int I(\lambda)\,d\lambda$, where $I(\lambda)$ is the observed spectrum.

center the fluorescent spectrum changes slowly compared to the instrumental resolution, so that each normalized measured spectrum converges to the normalized fluorescence spectrum, but near the line center the observed line is broadened by instrumental resolution. This can be seen in Fig. 1, where the 200-μm data are broadened relative to the 50-μm data at $|\Delta\lambda| < 3$ Å, while the 50-μm data are broadened relative to the 10-μm data at $|\Delta\lambda| < 1$ Å. At larger $\Delta\lambda$, each lower-resolution spectrum blends with the higher-resolution spectrum, indicating that the fluorescent spectrum is being observed in both measurements. For the line-wing data presented below, we have used a single curve that combines the 200-μm data at large $\Delta\lambda$, the 50-μm data at intermediate $\Delta\lambda$, and the 10-μm data at the smallest $\Delta\lambda$. No 10-μm data were taken for He, and Γ was obtained from the far-wing intensity since it had a Lorentzian wing in the region where the 50-μm slit width data was valid (see Figs. 2 and 3).

The emission spectra were measured for a number of noble-gas pressures between 100 and 1100 Torr; generally at 300, 600, and 900 Torr. If the spectrum corresponds to binary Rb*–noble-gas atom collisions only, then the far wing of the normalized emission from optically thin Rb will be proportional to the noble-gas density N. Thus we have plotted the normalized emission intensities divided by density (emission coefficient) in Figs. 2 and 3, since this will be independent of N for binary interactions. As can be seen, we observe no systematic N dependence of the emission coefficient for $|\Delta\lambda|$ greater than, typically, 3 Å. In the core of the line, however, the low-pressure lines are narrower and the emission coefficient increases with decreasing density. This can be seen best in the He data of Figs. 2 and 3, where the entire spectrum is shown. [If a single normalized Lorentzian line $I \propto \pi^{-1}\Gamma/(\Gamma^2 + \Delta k^2)$ with the half-width Γ proportional to N is plotted in this fashion the spectra for different pressures would blend at $\Delta k \sim 5\Gamma$ where the denominator is approximately Δk^2.] This emission coefficient is related to an absorption coefficient by Eq. (B5) of Ref. 3.

The experimental cell had a small but finite optical depth for wavelengths near the center of the resonance lines. Consequently radiation trapping attenuated the centers of the lines, normally by 5–15%. The line wings are not attenuated, so they appear slightly too intense relative to the integrated emission. The size of this effect is measured by measuring the ratio $I(\lambda_I)/\int I(\lambda)\,d\lambda$ as a function of Rb density at constant perturber density. Here λ_1 is some fixed wavelength on the far line wing and the total emission intensity $\int I(\lambda)\,d\lambda$ is used as the index of Rb density since it is almost proportional to Rb density at these low optical depths. In this manner it was found that the $I(\lambda_1)/\int I(\lambda)\,d\lambda$ ratio at the normal experimental Rb densities was 5–15% greater than the extrapolated limit at zero Rb density. From the measured $\int I(\lambda)\,d\lambda$ for any particular scan, this 5–15% correction could then be made.

A further correction of 10% per 100 Å for the relative detector sensitivity has also been applied to the data in Figs. 2 and 3. We infer from the scatter in this data that the typical accuracy of this corrected data is 10–20%.

Emission coefficients for $|\Delta k| < 1.5$ cm^{-1} have been plotted for the Ne, Ar, Kr, and Xe cases in Figs. 4 and 5. Unlike the He case, these data for the region close to line center were not included in Figs. 2 and 3.

Because of variations in spectrometer drive backlash, the shifts of the lines shown in Figs. 4 and 5 were measured by using the emission of an auxiliary Rb lamp as a reference during each scan. Shutters were alternately switched so as to intersperse the spectrum of that lamp and the cell spectrum during a single scan. The shifts at half-height thus obtained are given in Fig. 6 and the slopes of the fitted straight lines in Table I. The scatter in this shift data can be seen in Fig. 6, and is reflected in the uncertainties reported in Table I. At this accuracy no nonlinearity in shift versus density is apparent. A slight shift of the half-height center (~0.01 cm^{-1}) occurs as a result of the convolutions of hfs components of varying size with the Lorentzian broadening. This effect is smaller than the experimental scatter and has been neglected. These half-height shifts represent the shift of the Lorentzian core of the line for noble-gas pressures below an atmosphere. The breakdown of the impact approximation within the half-width will begin to influence the Xe shifts at about 700 Torr, the Kr shifts at about 1000 Torr, and the Ar shifts at slightly higher pressure.

In order to extract the Lorentz component of the linewidths from the data, allowance has to be made for the instrumental resolution and Rb hfs. For $|\Delta\lambda| < 1$ Å, the instrument resolution (~0.1 Å) at 10-μm slit width is insufficient to directly yield the fluorescent spectrum. Consequently, we have compared the data to convolutions of the instrument function with an assumed fluorescent spectrum. The fluorescent spectrum is taken to be a sum of four Lorentz and Doppler broadened (Voigt) components corresponding to the four resolved hyperfine components of the Rb resonance lines.[5] The amplitudes and centers of these components of the D_2 line are shown in Fig. 7; similar

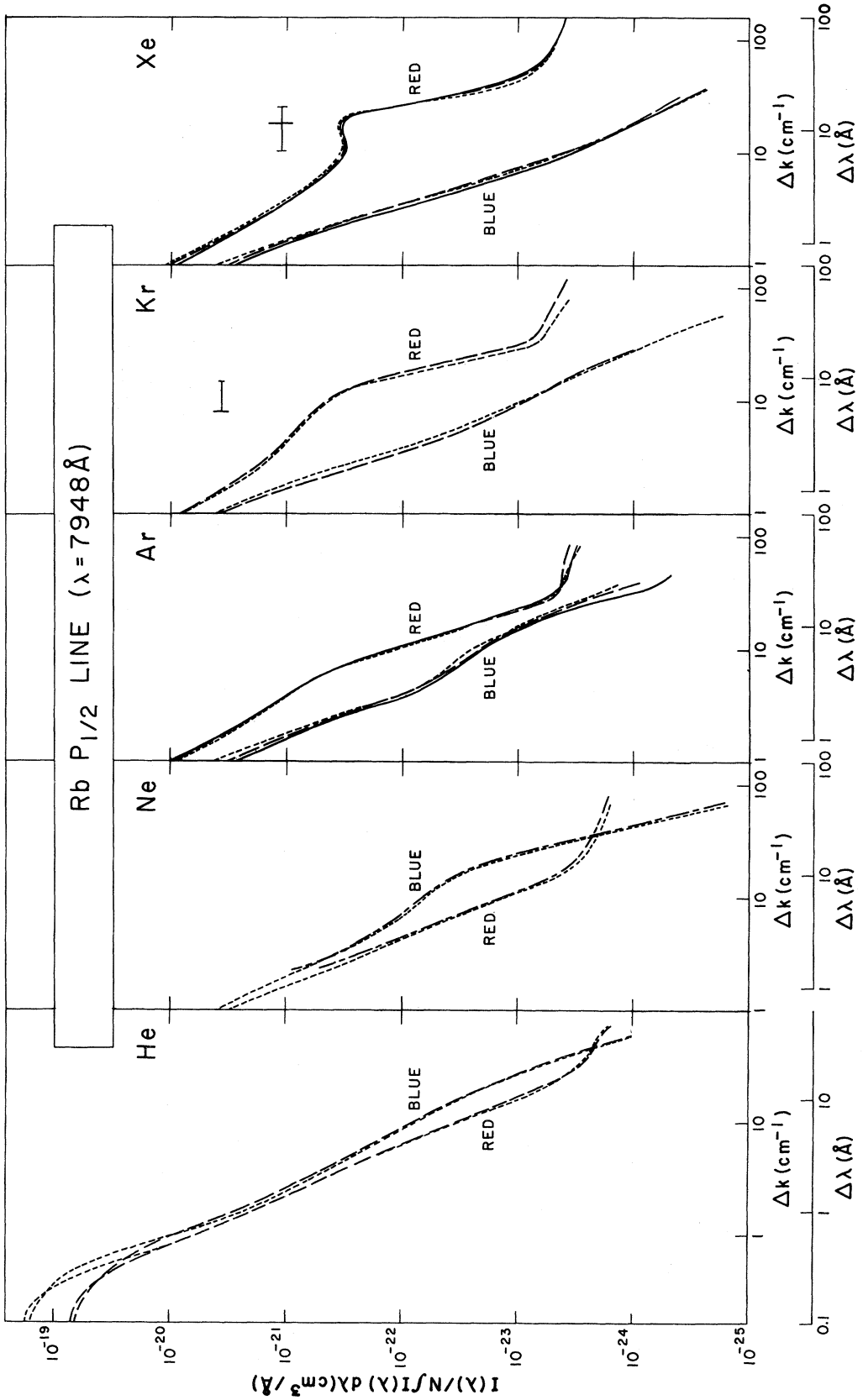

FIG. 2. Normalized emission spectrum divided by perturber density (emission coefficient) for the Rb $P_{1/2}$ (7948 Å) line perturbed by the noble gases. Data are shown for 150 Torr (— - — -), 300 Torr (- - -), 600 Torr (— —), and 900 Torr (——) perturber densities, equivalent to 0.17, 0.34, 0.68, and 1.02 r.d. units, respectively, at the cell temperature of 320 K (1 r.d. = $2.69\times10^{19}/cm^3$). $\Delta\lambda=\lambda-\lambda_0$ and $\Delta k=k-k_0$, where $k=\lambda^{-1}$ and λ_0 is the centroid of the unperturbed Rb resonance line. The bars above the Kr and Xe red satellites are the positions previously reported for these features (see text).

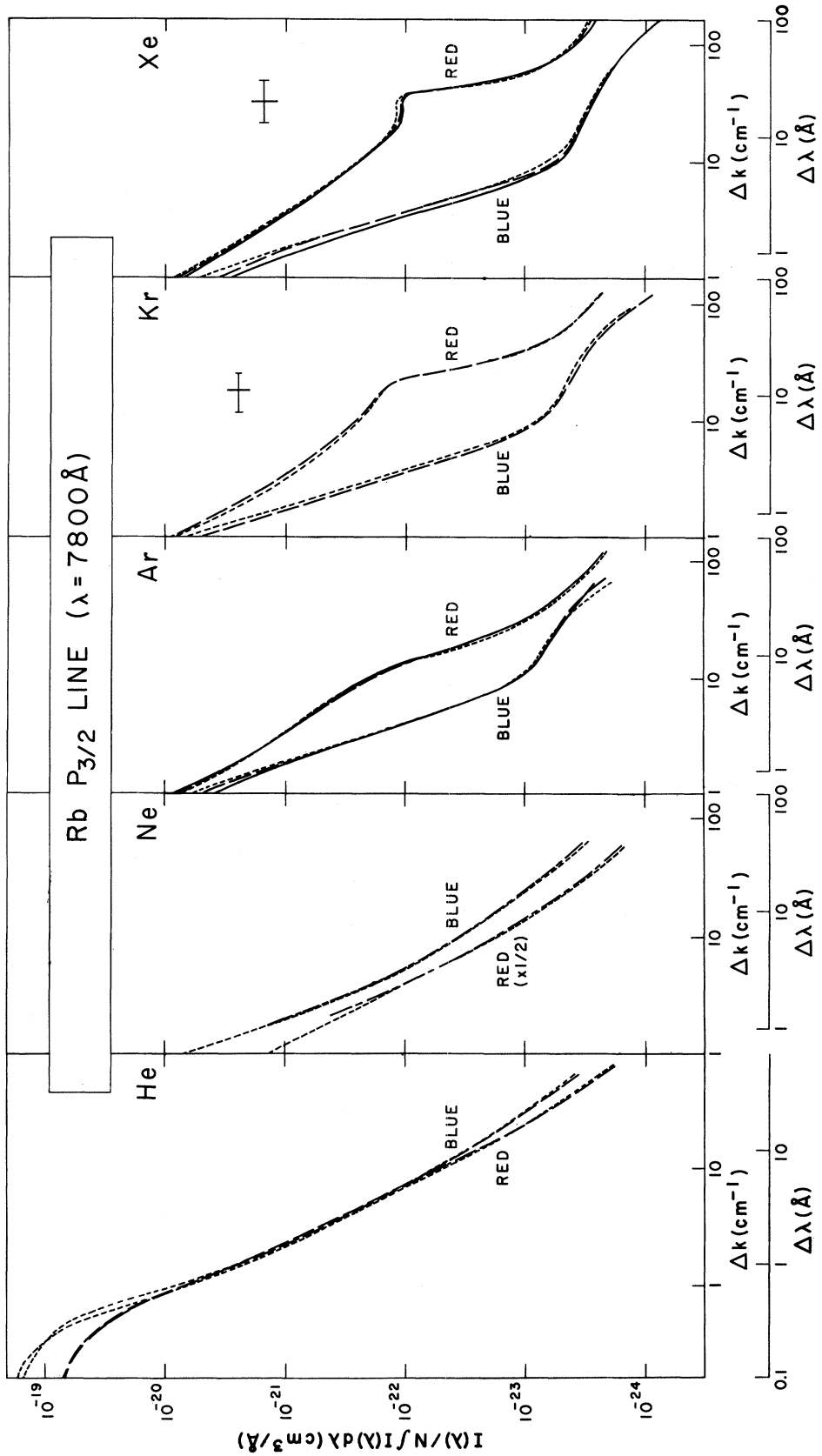

FIG. 3. Same as Fig. 2 for the Rb $P_{3/2}$ (7800 Å) line.

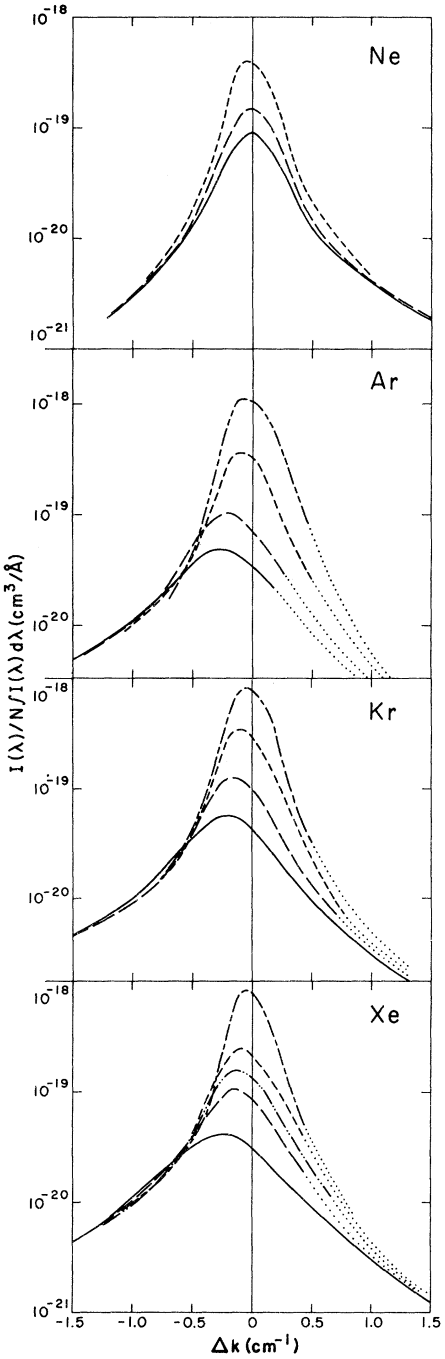

FIG. 4. Emission coefficient for the central region of the Rb $P_{1/2}$ (7948 Å) line perturbed by noble gases as observed with 10-μm spectrometer slits (~0.1 Å resolution); except for the 300-, 600-, and 900-Torr Xe data which were taken with 50-μm slits. Data are shown for 100 Torr (– – – –), 150 Torr (— – —), 300 Torr (– – –), 450 Torr (– · · –), 600 Torr (— —), and 900 Torr (——) perturber densities. In some cases where scanning irregularities occurred, dots are used to interpolate the blue-wing spectrum toward the intensities observed at larger $\Delta\lambda$ with 50-μm slits.

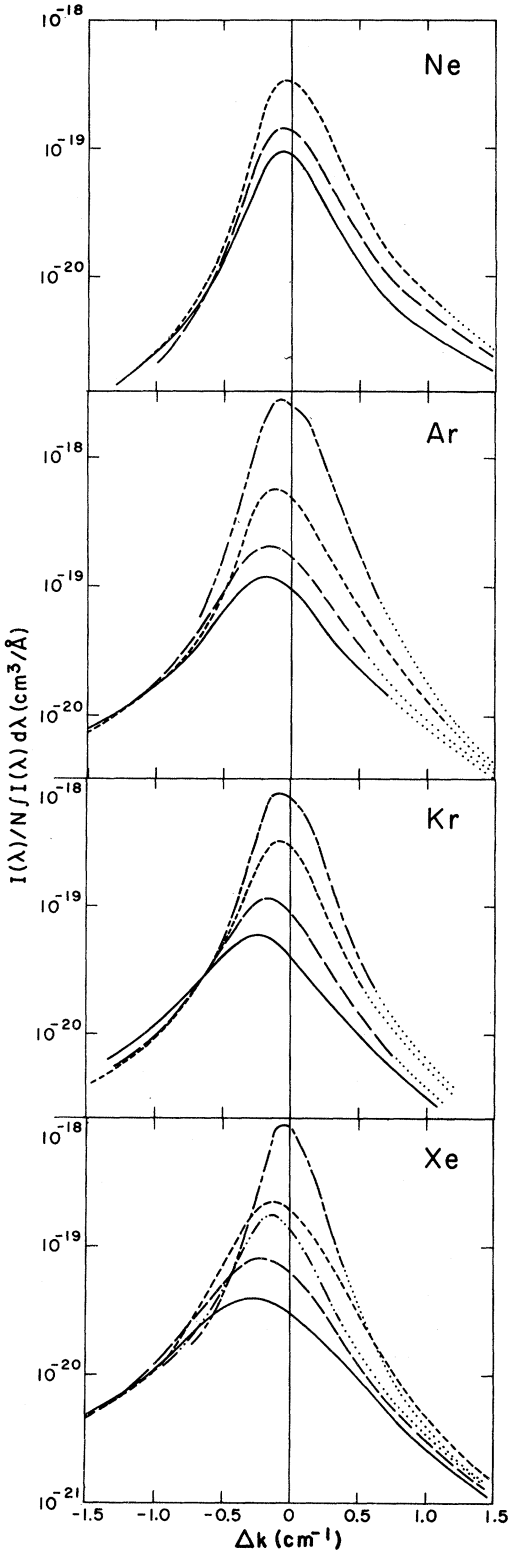

FIG. 5. Same as Fig. 4 for the $P_{3/2}$ (7800 Å) line. Again all scans were with 10-μm spectrometer except for 300, 600, and 900 Torr Xe which were with 50-μm slits.

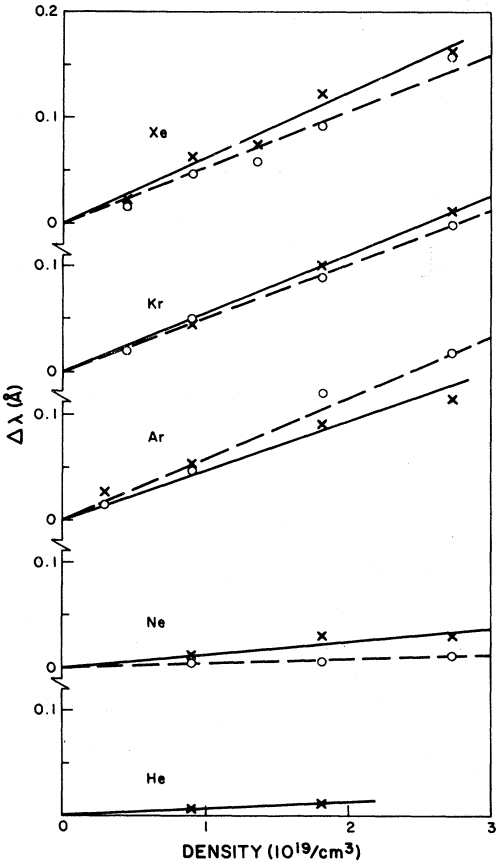

FIG. 6. Shifts of the line centers at half-height as a function of perturber densities. The (+) and solid lines refer to the $P_{3/2}$ (7800 Å) line, and the (○) and dashed lines to the $P_{1/2}$ (7948 Å) line.

separations occur for the D_1 line. The instrument function was measured by scanning narrow Kr lines at 7801 Å and 7853 Å from a lamp of slightly higher temperature than the experimental cell. Thus the recorded instrument function (cf. Fig. 7) is already a convolution of a Doppler source (~0.02-Å half-width) with the instrument function. Because of the similar masses and temperatures of Rb and Kr, almost the same Doppler width applies to each Rb line component. Therefore, the convolution of purely Lorentzian Rb hfs components with the measured instrument response represents the desired convolution of the four Doppler- and Lorentz-broadened (Voigt) lines with the instrument function:

$$S(k) = \int_{-\infty}^{\infty} dk' F(k-k')_{\mathrm{Kr}} I(k'), \qquad (1)$$

with

$$I(k') = \sum_{i=1}^{4} \frac{A_i \Gamma^2}{\Gamma^2 + (k' - k_i)^2},$$

where $F(k-k')_{\mathrm{Kr}}$ is the measured response to the Kr line, k_i is the centroid and A_i the intensity of each hyperfine component,[6] and $S(k)$ the measured Rb spectrum. One such set of convolutions is shown in Fig. 7, where it is compared to the Kr data from Fig. 4. The Γ values inferred from this comparison, and from similar comparisons for the other cases, are shown in Fig. 8. The results of comparisons of both 50- and 10-μm slit-width data with theoretical convolutions have been included in Fig. 8.

Note that the data in Fig. 7 diverge from Lorentzian at ~0.32 Å on the red wing at a height which rises with increasing pressure. This effect would leave no Lorentzian portion of the red wing above about 1100 Torr of Kr. This intrusion of the red wing into the Lorentz core is, compared to Kr, more rapid with Xe, less rapid with Ar, and barely seen for Ne. This relative importance of the non-Lorentzian red wings is expected, as explained in the conclusion. The widths given in Fig. 8 correspond only to the Lorentzian portion of the data.

III. COMPARISONS WITH PREVIOUS OBSERVATIONS

The positions of Rb-Kr and Rb-Xe red satellites and the shift and broadening of Rb lines have been reported by a number of authors. Some measurements were done at densities above 100 r.d.,[7] corresponding to a mean interatomic distance of less than 7 Å. Therefore they involve multibody interactions and should not be compared directly to the present low-pressure results. (To facilitate comparisons we will use traditional density units of relative density or r.d. One r.d. is the number density of a perfect gas at 760 Torr and 0 °C.) The shift and width of the Rb lines are also nonlinear at high perturber densities, with the nonlinearity appearing at lower densities for increasing noble-gas mass or polarizability. Thus we will attempt to find the low-pressure limits of previously reported shift and broadening rates for comparison with the present results.

The low-density limit of the red satellite positions and widths as reported by Chen and Fountain,[9] and by Jefimenko and Curtis,[10] are indicated in Figs. 2 and 3. It can be seen that the present results are in agreement insofar as satellite "positions" and "widths" can be assigned to barely resolved or unresolved features. The shape of the Rb-Xe satellite, appearing as a flat shoulder similar to our result, is also reported in Ref. 10. Some satellite intensity data have also been reported,[9] but not in a form that can be easily compared to absolute emission or absorption coeffi-

TABLE I. Low-pressure shifts and broadening. [a]

Perturber	Rb line	Shift (cm^{-1}/r.d.) Present (320 K)	Shift (cm^{-1}/r.d.) Other experiments		Shift (cm^{-1}/r.d.) Theory [g]	Broadening (cm^{-1}/r.d.) Present 2Γ (320 K)	Broadening (cm^{-1}/r.d.) Other experiments		Broadening (cm^{-1}/r.d.) Theory [g]
He	$P_{1/2}$(7948 Å)	...	$+0.24 \pm 0.06$ [b]	$+0.23$ [c]	+0.20	0.55 ± 0.1	0.59(0.51) [c]		0.72
He	$P_{3/2}$(7800 Å)	-0.022 ± 0.01		$+0.09$ [c]	+0.037	0.55 ± 0.1	0.74(0.64) [c]		0.53
Ne	$P_{1/2}$	-0.011 ± 0.01	$+0.06 \pm 0.12$ [b]	(0.00) [f]		0.28 ± 0.04		~0.33(0.31) [e]	
Ne	$P_{3/2}$	-0.06 ± 0.01		(−0.08) [f]		0.29 ± 0.05		~0.30(0.28) [e]	
Ar	$P_{1/2}$	-0.21 ± 0.02	-0.18 ± 0.06 [b]	(−0.19) [e]		0.54 ± 0.07	0.85(0.74) [c]	0.50(0.48) [e]	
Ar	$P_{3/2}$	-0.24 ± 0.035		(−0.24) [e]		0.55 ± 0.07	0.86(0.75) [c]	0.48(0.46) [e]	
Kr	$P_{1/2}$	-0.215 ± 0.015	-0.12 ± 0.06 [b]	(−0.17) [e]		0.54 ± 0.05			
Kr	$P_{3/2}$	-0.24 ± 0.015		(−0.20) [e]		0.48 ± 0.04			
Xe	$P_{1/2}$	-0.225 ± 0.02	-0.21 ± 0.06 [b]	−0.17 [d]		0.62 ± 0.07	0.53(0.46) [d]		
Xe	$P_{3/2}$	-0.27 ± 0.02		−0.20 [d]		0.63	0.53(0.46) [d]		

[a] The shifts correspond to the line center at half-height. For the present experiments only the Lorentz portion 2Γ of the full width is given; other cases correspond to the full half-height width. A density of 1 r.d. is $2.69 \times 10^{19}/cm^3$, corresponding to standard temperature and pressure. Numbers in parentheses correspond to the reported result adjusted to the temperature of the present experiment. The temperature dependence $T^{0.3}$ has been assumed to adjust the widths and the measured dependence from Refs. 11 and 14 to adjust the shifts.

[b] Reference 12. $T = 320$ K.

[c] Reference 15. $T \cong 510$ K. The nonlinearity in the Ar $P_{1/2}$ linewidth data has been reinterpreted as in Fig. 29 of Ref. 11 yielding 0.85 rather than 0.63 cm^{-1}/r.d. broadening.

[d] Reference 9. $T = 520$ K.

[e] Reference 11. Temperature dependence was measured typically from 420–770 K. The Ne broadenings correspond to a different interpretation of the linewidth data (Fig. 43) than used by the author. The Ar results are also given in Ref. 13.

[f] Reference 14.

[g] Reference 19.

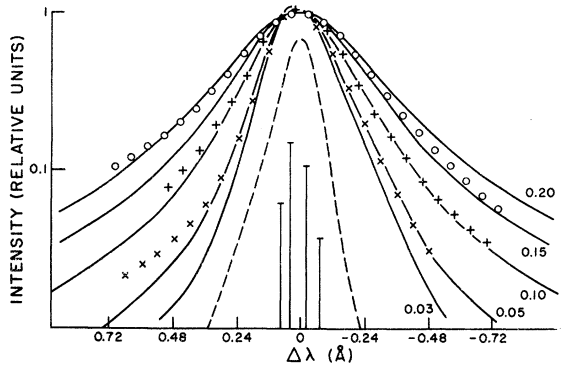

FIG. 7. Comparison of the Kr broadened, $P_{1/2}$ line, 10-μm slit-width data to theoretical convolutions given by Eq. (1). The dashed line is $F(k-k')$ of Eq. (1) in arbitrary units and the vertical lines are the four hfs components of the source spectrum, with relative intensities given on the log scale at the left. The solid lines are the theoretical convolutions [$S(k)$ in Eq. (1)] for the indicated values of Γ, in Å. The 300 Torr (×), 600 Torr (+), and 900 Torr (○) data from Fig. 4 are plotted for comparison. These data have been arbitrarily shifted vertically and horizontally to match the center and heights of the theoretical convolutions. The Γ values 0.05, 0.10, and 0.175, respectively, are inferred from this fitting procedure and plotted in Fig. 8. The portion of the red wings beyond $\Delta\lambda = 0.32$ Å rise above the theoretical convolution, indicating that the broadened line becomes non-Lorentzian here. This portion of the spectrum is not used in deducing the Γ of Fig. 8.

cients. Some of the above satellite position measurements were at higher temperatures than used here, but temperature should have little effect on the position.

In extrapolating shifts and widths measured at higher pressures to the low-pressure limit, nonlinearities are a problem. The shift has been shown to be nonlinear for Ar and Kr densities above about 2 r.d.[11] and we believe the width should be nonlinear as well. We believe that the cause of both of these nonlinearities is the intrusion of the non-Lorentzian wings into the Lorentzian core, as discussed in Sec IV. (It is customary to define the line center as the midpoint at half-height, and the width as that at half-height.) The present data were taken at densities of 0.15–1 r.d., and analyzed to identify the shift and width of the Lorentzian core of the line. Thus our data represent the zero density or impact broadening limit. The $P_{1/2}$-line shift data of Gershun *et al.*[12] were taken by a very-high-resolution magnetic scanning technique at 0–0.1 r.d. so these data also represent the zero-density limit. These data are given in Table I. It can be seen that they agree with the present results within the combined experimental uncertainties. Only the Kr

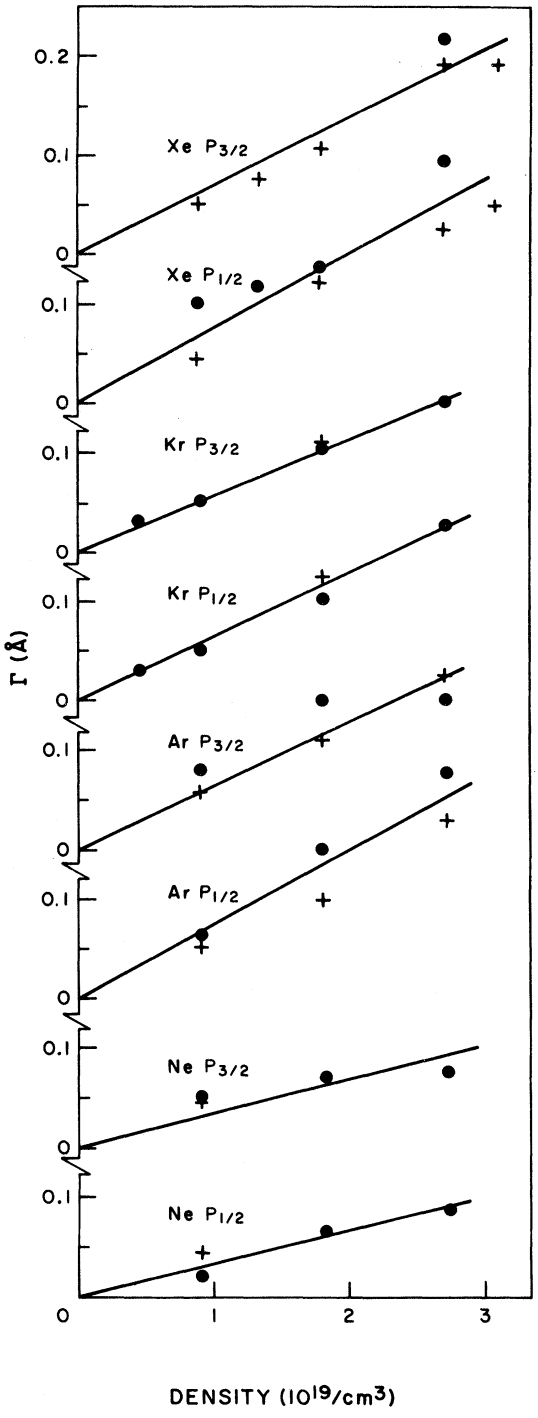

FIG. 8. Lorentzian half half-widths Γ as deduced by fitting the data of Figs. 4 and 5, and some additional 50-μm data, to theoretical convolutions given by Eq. (1). Figure 7 gives an example of this procedure. Widths obtained from 10-μm data are marked by (●), those obtained from 50-μm data by (+).

case is slightly outside the quoted estimated uncertainties.

Granier[11] has attempted to establish the zero-density of his observed shifts and widths, as well as is possible from data that normally extend from 3 to 50 r.d. He finds the widths to be linear for Ar perturber densities from 3–20 r.d. and nonlinear for Ne perturber densities from 2–15 r.d. The Ne line width given in Fig. 43 of Ref. 11 appears to be approaching ~1.5 cm^{-1} at zero Ne density, corresponding to an instrumental resolution of this size. Thus the nonlinearity of the Ne broadening appears to be due to the convolution of an instrumental width of about 1.5 cm^{-1} with a linewidth that broadens fairly linearly to about 5 cm^{-1} at 15 r.d. (the highest-pressure data point in Fig. 43). Since our line-shape data lead us to expect linear broadening rates for He and Ne perturbers up to even higher densities, we interpret Fig. 43 of Ref. 11 as consistent with a constant Ne broadening rate of about 0.33 cm^{-1}/r.d. (5 cm^{-1} at 15 r.d.) for the $^2P_{1/2}$ line and slightly less for the $^2P_{3/2}$ line. These inferred values are indicated in Table I. Neon broadening rates of 0.15 cm^{-1}/r.d. for both Rb lines are given in Table IX of Ref. 11, apparently from a different interpretation of the data of Fig. 43. The temperature of Granier's measurement was 415 K, so this broadening rate might be expected to decrease 10–15% at our temperature of 320 K. (The theoretically expected temperature dependence $T^{0.3}$ for a Van der Waals interaction has been supported by Granier's measurements. We do not expect this to be exact, but use it here and below as a best guess for these minor adjustments.) Granier's argon broadening rates are also given in Table I, from the linewidths of Ref. 13. These widths are the result of Granier's subtraction of an assumed red satellite shape from the resonance line, with the resultant broadening only some 60% of that in the original data. This broadening was measured at a temperature of 375 K, so a 5–10% decrease might be expected at 320 K. Thus Granier's Ne (as reinterpreted) and Ar broadening rates both appear to be about 15% below the present results, which is well within the combined experimental uncertainties. Krypton broadening rates of 0.30 and 0.36 cm^{-1}/r.d. are reported in Ref. 11. These broadening rates are grossly inconsistent with our results, and we suspect that the discrepancy is probably due to a failure to allow for the instrumental width in interpreting linewidth data of the type in Fig. 43 of Ref. 11. No Kr broadening data are shown in Ref. 11 so we cannot verify this supposition, and we have not included these broadening rates in Table I.

The line shifts observed by Granier at densities from 3–30 r.d. are clearly nonlinear with perturber density for Ar and Kr perturbers (Ref. 13 and Figs. 29 and 41 of Ref. 11), but the zero-density shift per r.d. has been obtained from the data (Tables III and V of Ref. 11). From temperature dependence measured by Granier these 370-K shifts should be about 5% lower at our 320 K temperature. These low-density shift rates are given in Table I, where it can be seen that they are in excellent agreement with the present data. For Ne, Granier[11,14] obtained strongly temperature-dependent low-density shift rates at 410, 570, and 770 K, but these rates extrapolate smoothly to the 320-K values given in Table I, which are again in agreement with the present results (these small shifts have a greater fractional uncertainty).

Chen and co-workers have also measured the shifts and widths due to He, Ar, and Xe perturbers.[9,15] The Xe measurements were at densities of 0.5–3 r.d. Since we expect departure from linear shift and width to start at about 1 r.d., the departures should not be very large for these data. The experimental temperature for observation of absorption shifts and widths is typically 100–150 °C, so that these widths and shifts could be expected to decrease by about 10% at our 50 °C temperature. Thus the Xe shift and broadening rates from Ref. 9, as reported in Table I, are about 30% below what would be expected from our data. Any allowance for the expected nonlinearity above 1 r.d. would increase this difference which, although moderate, appears to be systematic. It is not clear if allowance was made in Ref. 9 for contributions of the Rb hfs and the spectrometer instrumental width.

The shift data of Chen[15] for Ar are consistent with those of Granier (Fig. 27 of Ref. 11 or Ref. 16) but no subtraction of the red satellite from the line was made. As noted above, this yields apparent broadening rates from 0–10 r.d. of about 0.85 cm^{-1}/r.d. for both lines rather than the ~0.5 cm^{-1}/r.d. reported by Granier in Refs. 11 and 13. If these 520-K broadening rates are decreased by $T^{0.3}$ to 0.75 cm^{-1}/r.d. for comparison with our 320-K rates, they are ~40% greater than our results (Table I). We would in fact expect them to be 10–20% greater due to the predicted nonlinearity that set in at ~1 r.d. Thus our broadening rate is about midway between those obtained by interpreting the ~10 r.d. data with and without satellite subtraction as in Refs. 11 and 13, respectively. It is probable that the satellite does increase the width at the densities of these experiments, but since the assumed satellite at ~4 cm^{-1} is no more than a change in the slope of the low-pressure

wing intensity (Fig. 2), the satellite shape in any subtraction would appear to be underdetermined.

Finally, the He data given in Table I can be considered. We expect the He induced shifts and widths to be linear to very high densities, which is consistent with the data of Chen.[15] These broadenings and shifts then require only temperature correction for comparison with the present data. The $T^{0.3}$ corrected widths are then in reasonable agreement with the present data. The temperature dependences of the He induced shifts are unknown. While the $P_{3/2}$ line shifts of Chen[15] and of the present work disagree substantially, a temperature dependence similar to that measured by Granier[14] for the $P_{1/2}$ line shift due to Ne could easily explain the difference. Note, however, that the 520-K He $P_{1/2}$ line shift of Chen[15] agrees with that of Gershun *et al.*[12] at 320 K. Thus very little temperature dependence is seen for the shifts of the $P_{1/2}$ line due to He perturbers and of the $P_{3/2}$ line due to Ne perturbers. A $T^{0.3}$ dependence is reported[11] for both lines due to Ar and Kr perturbers, and rapid variations[14] are reported for the $P_{1/2}$ line due to Ne perturbers. Comparison of the present results with Ref. 15 indicates similarly rapid variations for the $P_{3/2}$ line due to He perturbers.

IV. CONCLUSIONS

The present measurements of the low-pressure Rb–noble-gas spectra extend our earlier quantitative measurements of the far-wing intensities[4,17] to line center. It is hoped that these extensive data, combined with a considerable amount of information regarding the Rb–noble-gas interaction potentials,[18] will provide a valuable testing ground for realistic theories of pressure broadening. A realistic treatment of the impact broadening of Rb by He has recently been carried out[19]; the results are given in Table I. We are aware of only two other calculations for the Rb case, one which incorrectly used the quasistatic theory to calculate the broadening,[20] and the other which simply uses the data to fix cross-section parameters in the theory.[11] We have not attempted to compare the wings with quasistatic spectra based on Pascale and Vanderplanque potentials,[18] since the satellite shapes and other near-wing features of the present data require dynamical corrections to a quasistatic analysis.[21–26] In addition, the $P_{1/2}$ line is due to a single isolated $A^2\Pi_{1/2}$ state, whereas the $P_{3/2}$ line comes from the $A^2\Pi_{3/2}$ and $B^2\Sigma_{1/2}$ adiabatic states arising from the $5^2P_{3/2}$ state. At the internuclear separation responsible for the present data we believe that these $A^2\Pi_{3/2}$ and $B^2\Sigma_{1/2}$ states will be nonadiabatically mixed [$B^2\Sigma_{1/2}(R) - A^2\Pi_{3/2}(R) < h/\tau_c$ where τ_c is a representative collision duration]. Thus the quasistatic approximation, based on the classical Franck-Condon principle for adiabatic states, will probably not be a valid approximation for the $5^2P_{3/2}$-$5^2S_{1/2}$ line.

The line-center spectra in Figs. 4 and 5 indicate clearly why other authors observed a nonlinearity of line shift. The non-Lorentzian wing of the line rises in proportion to density but the line peak does not. Once the non-Lorentzian red wing merges above 50% of the line peak the line center at half-height shifts more rapidly. For example, the transition to non-Lorentzian shape occurs at ~0.32 Å in Fig. 7; so that for $\Gamma > 0.32$ Å the half-height shift will become nonlinear. The onset of nonlinearity will occur at a density of roughly 1 r.d. for the Ar, Kr, and Xe cases shown. On the other hand, the blue wings for Ar, Kr, and Xe perturbers have fallen below Lorentzian by 1 Å (see Figs. 2 and 3). This will have the effect of further increasing the net red shift at half-height for densities that yield $\Gamma > 1$ Å (above ~4 r.d.). Clearly this increased spreading of the red wing and decreased spreading of the blue wing will also influence the linewidth and asymmetry. Since no broadening measurements have covered the entire 0–20 r.d. region, the net effect on linewidth can only be inferred by comparing, for example, our low-pressure Rb-Ar broadening data to those of Chen[15] reported in Table I. The accompanying asymmetry of the line has been reported in Ref. 15.

Virtually all calculations of a pressure-broadened spectrum near the line center but beyond the impact regions have used power-law interaction potentials. Holstein was the first to calculate line shapes due to straight-line paths in a power-law interaction potential, using Fourier analysis of the semiclassical oscillator, but only a summary of the results was published.[21] However, Anderson and Talman[22] and more recently Tvorogov and Fomin[23] have analyzed the same problem with similar assumptions and methods and have arrived at similar results. For an attractive Van der Waals interaction ($\Delta V \propto -C_6R^{-6}$) each of these treatments yields a far red-wing intensity that varies as $\Delta k^{-3/2}$, in agreement with the quasistatic theory. Holstein and Tvorogov and Fomin obtain a far blue-wing intensity that varies as the product of $\Delta k^{-7/3}$ and an exponential factor while Anderson and Talman reduce their expression to only an exponential. The $\Delta k^{-7/3}$ dependence without the additional factor was obtained by Lindholm[24] by a more approximate method.

Holstein[21] gives an expression for the frequency shift $\Delta\omega$ at which the quasistatic contribution to

the red wing equals the impact contribution, and notes that it is equal to the familiar $\Delta\omega_c \cdot \tau_c = 1$ where τ_c is the "collision time." The usual validity criterion for the impact approximation is $\Delta\omega \cdot \tau_c \ll 1$; so one expects a transition to a Lorentz profile inside this $\Delta\omega_c$, which is often called the "Weisskopf frequency." (The "far" wings refer to well beyond this transition zone.)

In the present case we expect the long-range Rb–noble-gas interaction to be attractive for the Ar, Kr, and Xe cases, with the Rb*(5p) interaction more attractive than for Rb(5s).[18] The Ar, Kr, and Xe interactions apparently follow the Van der Waals (C_6R^{-6}) form only at very long range,[18] and have diverged considerably at the internuclear separations responsible for most of the impact broadening and the adjacent line wings. Nonetheless, the general behavior and range of the resultant difference potentials are similar to those obtained by considering only a C_6R^{-6} difference potential with the C_6 constants given by Baylis.[18] Thus it is interesting to compare the present Ar, Kr, and Xe line-shape data to the results of the above theories for $\Delta V \propto C_6R^{-6}$. For this comparison, we have made (straight line) power-law fits to the near-wing data of Figs. 2 and 3, where the fitted regions are chosen by requiring that a single power law fit the data. The resulting powers and fitted regions are reported in Table II for all perturber cases, including He and Ne. (Note: this procedure can only be used outside a few half-widths because even a Lorentzian does not go as Δk^{-2} close to the line center.)

For He and Ne perturbers the interactions bear little connection to the Van der Waals interaction since the latter is so weak. We expect in these cases that the higher collision velocities and close-range interactions will lead to a shorter τ_c or larger $\Delta\omega_c$. This is in fact seen since the wings fall off quadratically out to quite large $\Delta\lambda$ in these cases (Table II). Divergence from this "impact" shape on both wings only occurs beyond about 10 Å, with no indication of a transition to $\Delta\lambda^{-3/2}$ or $\Delta\lambda^{-7/3}\exp(-c\Delta\lambda^{5/6})$. By the time $\Delta\lambda$ is large enough to invalidate the impact approximation, the Rb-He and Rb-Ne interaction potentials for these large $\Delta\lambda$ are far from Van der Waals behavior so no $\Delta\lambda^{-3/2}$ region is seen. For Ar, Kr, and Xe on the other hand, the $\Delta\lambda = 1$–5 Å regions of the red wings fit the $\Delta\lambda^{-3/2}$ behavior reasonably well, indicating that a negative ΔV with roughly R^{-6} behavior is responsible for these red-wing regions.

The blue wings appear to fall off approximately as $\Delta\lambda^{-3}$ beyond 1 Å for Kr and Xe, as was observed by Chen and Phelps for Cs-Ar.[25] Our Rb-Ar blue wings appear to be midway between the $\Delta\lambda^{-2}$ and impact $\Delta\lambda^{-2}$ behavior, as might be expected for a transition case, while the He and Ne blue wings are nearly Lorentzian to $\Delta\lambda \sim 10$ Å (a blended satellite for $P_{1/2}$ perturbed by Ne obscures this wing behavior beyond 4 Å).

It is interesting to compare the observed wavelengths $\Delta\lambda_{qs}$ corresponding to the transitions from impact ($\Delta\lambda^{-2}$) to quasistatic ($\Delta\lambda^{-n}$, $n \neq 2$) shapes with Holstein's $\Delta\omega_c$, the red-wing transition frequency. These $\Delta\omega_c$, expressed as $\Delta\lambda_c$ in Å units, are given in Table II, where we have used a $\Delta V = -C_6R^{-6}$ with C_6 obtained from the difference between the Van der Waals coefficients given by Baylis[18] for the Rb(5 ^2P_J) and Rb(5 $^2S_{1/2}$) interaction with the noble gases. (We have ignored the effect of the fine structure and used a single C_6 for both ^2P states. Then $\Delta\omega_c$ is given by Holstein as $v^{6/5}C_6^{-1/5}$ where v is the collisional velocity, taken here as the average thermal velocity.) In the

TABLE II. Power law ($I \propto \Delta k^{-x}$) fits to the near-wing intensities.

Rb line	Perturber	x for red wing	Fitted $\Delta\lambda$(Å) region of red wing	x for blue wing	Fitted $\Delta\lambda$(Å) region of blue wing	$\Delta\lambda_c$ [b] (Å)
$P_{1/2}$ (7948 Å)	He	2.0	1–20	1.9	1.5–12	9.5
$P_{3/2}$ (7800 Å)	He	2.2	1–12	2.1	1–8	9.5
$P_{1/2}$	Ne	2.5	0.6–8	2.0	0.6–3.5	3.5
$P_{3/2}$	Ne	2.4	0.6–8	2.4	0.6–8	3.5
$P_{1/2}$	Ar	1.6	1–3.5	~2.8	0.8–2.5	1.9
$P_{3/2}$	Ar	1.4	1.3–6	2.8	1–4.5	1.9
$P_{1/2}$	Kr	(a)	(a)	3.2	0.8–3	1.4
$P_{3/2}$	Kr	1.5	1–4	3.0	1–4	1.4
$P_{1/2}$	Xe	1.5	1–4	3.1	1–7	1.1
$P_{3/2}$	Xe	1.5	0.8–6	3.2	1.5–7	1.1

[a] A blended red "satellite" at 4–8 Å dominates this near-wing shape.

[b] $\Delta\lambda_c$ is the transition wavelength from the Lorentzian $\Delta\lambda^{-2}$ to quasistatic $\Delta\lambda^{-3/2}$ dependence of the red wing, from Ref. 21.

interest of completeness we have included the He and Ne cases, although as noted above the Van der Waals interaction is not very relevant in these cases. The surprisingly good agreement between the experimental [$\Delta\lambda_{qs}$(He) = 12–20 Å, $\Delta\lambda_{qs}$(Ne) $\cong$ 8 Å], and calculated [$\Delta\lambda_c$(He) = 9.5 Å, $\Delta\lambda_c$(Ne) = 3.5 Å] for these cases is attributed to the fact that the Van der Waals interaction apparently yields about the right interaction distance. For the Ar, Kr, and Xe cases the fitted regions reported in Table II generally start at $\Delta\lambda \cong 1$ Å, which is simply the beginning of the data being fitted. Thus $\Delta\lambda_{qs} \leq 1$ Å for these cases and convolution comparisons are necessary to identify $\Delta\lambda_{qs}$. As has been previously noted, a $\Delta\lambda_{qs} \cong 0.32$ Å can be identified in Fig. 7 for the $P_{1/2}$ red wing perturbed by Kr. As expected, we find from similar comparisons to theoretical convolutions that this red-wing transition occurs somewhat closer to line center for Xe and further for Ar perturbers. Thus the theoretical $\Delta\lambda_c$ in Table II appear to be about a factor of 3 too large. The experimental wavelengths corresponding to transitions away from the impact ($\Delta\lambda^{-2}$) shape for the blue wings due to Ar, Kr, and Xe perturbers are not well established by the data since this is very sensitive to the instrumental resolution and some scanning hysteresis problems that plagued the experiment. Our rough estimate is that this transition occurs at about 1 Å for these blue wings. For He and Ne perturbers this transition occurs near the outer limit of the fitted regions reported in Table II (i.e., from 4–12 Å).

More detailed comparison can be made to the theoretical intensities, as has been done in Ref. 25 for Cs-Ar, but in view of the ambiguity in the meaning of C_6, the poor blue-wing fit obtained in Ref. 25 and uncertainty in ranges of validity of the theoretical expressions, the usefulness of such comparisons is not apparent. It must be emphasized that these power-law dependences are of very limited value in predicting wing intensities, since divergence from Van der Waals interactions[18] and the resultant spectra can occur at quite small energy shifts and the far wing intensities bear no relation to these simple power laws.

---

*This work was supported in part by the Air Force Weapons Laboratory under contract AFWL-74-09 and by the Advanced Research Project Agency under contract DAHC04-73-C-0029.

†Visiting Fellow, 1973-74, on leave from Max-Plank-Institut für Strömungsforschung, Göttingen, Germany.

‡Staff member, Laboratory Astrophysics Division, National Bureau of Standards.

[1]S. Y. Chen and M. Takeo, Rev. Mod. Phys. 29, 20 (1957).

[2]J. R. Fuhr, W. L. Wiese, and L. J. Roszman, *Bibliography on Atomic Line Shapes and Shifts*, Natl. Bur. Stand. Spec. Publ. 366 and 366, Suppl. 1 (U.S. GPO, Washington, D.C., 1972).

[3]R. E. Hedges, D. L. Drummond, and A. Gallagher, Phys. Rev. A 6, 1519 (1972).

[4]D. L. Drummond and A. Gallagher, J. Chem. Phys. 60, 3426 (1974).

[5]A. Gallagher and E. L. Lewis, J. Opt. Soc. Am. 63, 864 (1973).

[6]The A_i used correspond to fluorescence from Rb vapor that is pumped by white light. This yields the same set of A_i as obtained from an optically-thin thermal source in which the population of every excited sublevel (F, m_F) is equal. For $T \geq 300$ K the collisional hyperfine mixing due to noble-gas collisions will yield these intensities if the total excited ^{85}Rb and ^{87}Rb correspond to the isotopic ratios.

[7]J. Robin and S. Robin, C. R. H. Acad. Sci. B 233, 1019 (1951).

[8]S. Y. Chen, R. B. Bennett, and O. Jefimenko, J. Opt. Soc. Am. 46, 182 (1956).

[9]S. Y. Chen and C. W. Fountain, J. Quant. Spectrosc. Radiat. Transfer 4, 323 (1964); M. Takeo and S. Y. Chen, J. Quant. Spectrosc. Radiat. Transfer 4, 471 (1964).

[10]O. Jefimenko and W. Curtis, J. Chem. Phys. 27, 953 (1957).

[11]R. Granier, Ann. Phys. (Paris) 4, 383 (1969).

[12]V. V. Gershun, V. Khutorschikov, and N. N. Yakobson, Opt. Spektrosk. 31, 866 (1971) [Opt. Spectrosc. 31, 470 (1971)].

[13]R. Granier and J. Granier, C. R. Acad. Sci. B 262, 761 (1966).

[14]R. Granier and J. Granier, C. R. Acad. Sci. B 262, 1502 (1966).

[15]S. Y. Chen, Phys. Rev. 58, 1051 (1940).

[16]R. Granier, J. Granier, and E. De Croutte, J. Phys. (Paris) 24, 349 (1963).

[17]C. G. Carrington and A. Gallagher, Phys. Rev. A 10, 1464 (1974).

[18]W. E. Baylis, J. Chem. Phys. 51, 2665 (1969). A more complete and accurate calculation by this approximation method is that of J. Pascale and J. Vanderplanque, J. Chem. Phys. 60, 2278 (1974).

[19]E. Roueff and A. Suzor, J. Phys. (Paris) 35, 727 (1974).

[20]L. Klein and H. Margenau, J. Chem. Phys. 30, 1556 (1959).

[21]See Sec. V of Ref. 25 for references to unpublished work by T. Holstein. An incomplete summary has been reported in: T. Holstein, Phys. Rev. 79, 744 (1950).

[22]P. W. Anderson and J. D. Talman, Bell Tel. Syst., Tech. Publ. No. 3117 (1956).

[23]S. D. Tvorogov and V. V. Fomin, Opt. Spektrosk. 30, 418 (1971) [Opt. Spectrosc. 30, 228 (1971)].
[24]E. Lindholm, Ark. Mat. Astron. Fys. 32A, 1 (1945).
[25]C. L. Chen and A. V. Phelps, Phys. Rev. A 7, 470 (1973).
[26]K. M. Sando and J. C. Wormhoudt, Phys. Rev. A 7, 1889 (1974); K. Sando, Phys. Rev. A 9, 1103 (1974).